Energy Engineering

Tech Science Press

Doi:10.32604/ee.2025.073542

ARTICLE

Distributed Iterative Learning Control for Load Balancing in Flexible AC/DC Hybrid Distribution Systems

Hong Zhang[1], Bin Xu[1], Jinzhong Li[1], Xiaoxiao Meng[2,*], Cheng Qian[2], Wei Ma[1] and Yuguang Xie[1]

[1]State Grid Anhui Electric Power Co., Ltd., Electric Power Research Institute, Hefei, 230601, China

[2]Anhui Provincial Key Laboratory of Renewable Energy Utilization and Energy Saving, Hefei University of Technology, Hefei, 230009, China

*Corresponding Author: Xiaoxiao Meng. Email: mxxfreedom@hfut.edu.cn

Received: 20 September 2025; Accepted: 03 December 2025; Published: 27 April 2026

ABSTRACT: The increasing integration of distributed renewable energy sources in the distribution network leads to unbalanced load rates in the distribution network. The traditional load balancing methods are mainly based on network reconfiguration, which have problems such as a long time scale and poor adaptability. In response to these issues, this paper proposes a distributed iterative learning control (ILC) strategy for load balancing in flexible AC/DC hybrid distribution systems. This method combines the consensus algorithm with the ILC mechanism to construct a multi-terminal AC/DC flexible interconnection system model. It is only necessary to measure the load rate of adjacent units without observing the overall system status, which greatly reduces complexity and enhances robustness. In this paper, a new energy photovoltaic and energy storage integrated system was built through MATLAB/Simulink simulation, and the effectiveness of the proposed strategy under normal working conditions and port faults was verified through this system. Through comparative studies with event-triggered control and traditional consensus algorithms, as well as real-time simulations on the RT-LAB simulation platform, it has been confirmed that this method has superior performance in terms of convergence speed, steady-state accuracy, and dynamic response, and has the potential to be applied in practical models. It is suitable for application in medium and low voltage distribution systems with new energy access.

KEYWORDS: AC/DC hybrid distribution systems; iterative learning algorithm; load rate

1 Introduction

In recent years, the proportion of distributed renewable energy access in distribution networks has been greatly increased, and traditional passive distribution networks are rapidly transforming into active distribution networks [1]. The integration of large-scale renewable energy into distribution networks has played a positive role in alleviating energy crises and addressing environmental issues [2]. However, the high penetration rate of distributed renewable energy has also introduced problems such as voltage fluctuations, decreased power supply reliability, and deteriorating power quality in distribution networks [3]. Intermittent energy sources, including wind and photovoltaic power, can also cause sharp fluctuations in feeder power, which severely limits their access capacity in distribution networks [4]. In an active distribution network, the abundance of renewable energy, the level of economic development, and the current-carrying capacity along each feeder line differ, which results in variations in the penetration rate of distributed renewable energy and the load level among different feeders. The unevenness and fluctuation of distributed generation (DG) and load distribution on the feeder will lead to the imbalance of feeder power, which reduces the utilization efficiency of network assets and even causes network congestion [5]. Therefore, the problem of

unbalanced load on active distribution network feeders with a high proportion of renewable energy needs to be resolved [6]. At present, many studies are being conducted on the load balancing problem of distribution networks. However, most of these works adopt the method of network reconfiguration to transfer the load from heavy- to light-load feeders [7]. Reference [8] minimized load balancing indicators, active power loss, and node voltage deviation through network reconfiguration. This study proposed a chaotic interference beetle antenna search algorithm to reduce the computing time, but it ignored the high proportion of distributed energy sufficiently. Refs. [9,10] constructed a multi-objective network reconfiguration model and considered the output of distributed power sources simultaneously. However, its time scale is relatively long, which causes difficulty in adapting to the strong randomness of high-proportion distributed power sources. Reference [11] combined the multi-objective fuzzy algorithm with the ant colony algorithm to optimize the DG distribution. This approach reduces losses and improves the load balancing of the feeder. However, owing to the limitation of the operation frequency of the segmented switch [12], the time scale of network reconfiguration is generally long. This method is also unsuitable for distributed power sources with strong randomness. For this reason, it is necessary to adopt a new control method to achieve load rate balancing control in the distribution network.

On the other hand, iterative learning control, as an advanced control method, has long been applied in the field of AC/DC microgrids. Reference [13] systematically reviewed the origin of iterative learning control and provided a comprehensive overview of the field, laying a solid theoretical foundation for this control method. Reference [14] proposed an adaptive iterative learning control method for a class of nonlinear strict feedback systems, effectively enhancing the tracking performance and control accuracy of the system in repetitive running tasks. Reference [15] applied model-free adaptive iterative learning control to the secondary frequency regulation of microgrids, demonstrating its ability to perform data-driven control for complex systems. Reference [16] proposed a novel distributed iterative learning secondary control strategy to enhance the recovery accuracy of voltage and frequency in AC microgrids. Reference [17] explored the application of iterative learning control in production-consumption DC microgrids, aiming to optimize power distribution.

Reference [18] has leveraged its periodic learning capability to effectively suppress frequency deviations caused by the fluctuations of distributed energy resources. Reference [19] has developed distributed or adaptive ILC strategies to enhance the dynamic performance of voltage regulation in multi-inverter parallel systems. ILC has also been employed to achieve more precise power sharing [20] and to coordinate the charging/discharging processes of energy storage systems [21]. These works have collectively established a robust control framework [22], proving the effectiveness and robustness of ILC in addressing control challenges with repetitive operational patterns in microgrids [23]. However, although iterative learning control has been widely applied in microgrids [24], its potential in solving the load rate balancing problem of active distribution network feeders remains unexplored. Based on this, this article makes the following contributions. Firstly, we propose a new distributed control architecture that integrates the traditional consistency algorithm with the ILC mechanism. This design essentially does not require a specific model. It only needs local feeder load rate measurements from adjacent units, thereby eliminating the reliance on an accurate global system model and significantly enhancing its practicality and robustness. Secondly, the proposed strategy introduces a fast convergence mechanism. By utilizing the historical adjustment experience accumulated by periodic iterative learning, the control system is able to dynamically optimize its output. This enables the feeder load rate to converge to a balanced state in an extremely short time, and its performance far exceeds the minute or longer time scale required for traditional network reconfiguration. Finally, we have built multi-scenario robustness guarantees into the framework. Even in the event of unexpected situations such as the disconnection of the slave control port or the master control port, the

system can still maintain normal operation. This is achieved through dynamic control mode switching strategies (such as switching from PQ mode to VF mode) and effective isolation of faulty nodes, thereby ensuring the operational resilience of the remaining network. In conclusion, this paper not only innovatively applies ILC to the specific problem of feeder load balancing, but also provides a comprehensive solution, effectively addressing the core limitations of existing methods in terms of speed, model dependency, and robustness.

2 System Structure and Basic Control Strategies

2.1 System Structure

Fig. 1 shows the basic structure of the flexible AC/DC distribution network. This network consists of N AC power sources, L DC power sources, and accordingly, N converters (VSCs) and L DC transformers (DCTs). Among them, R_{sk} and L_{sk} represent the line impedance of the AC line, and R_{dcL} represents the line resistance of the DC line. All flexible converters share one common DC bus.

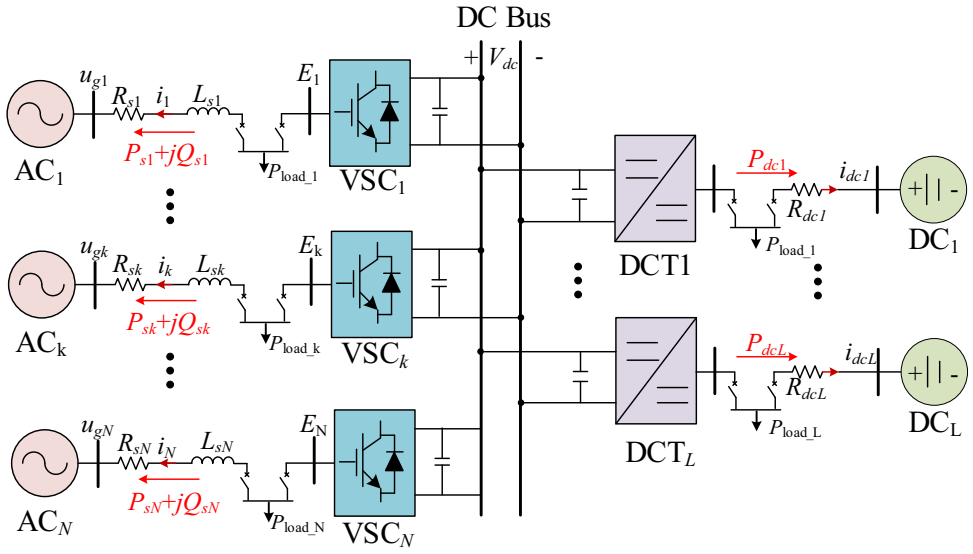

Figure 1: Topology of a multi-terminal AC/DC distribution network with flexible interconnections

2.2 Basic Control for the Converters

For the local control of all converters in the topological structure, this study employs a master–slave control architecture. One VSC is selected as the master unit, and $V_{dc}Q$ control is applied to it, while the remaining VSCs operate under conventional PQ control. Regarding the DC-side slave control for DCTs, the local control strategy adopts the widely recognized DAB single-phase shift control method, which ensures stable transmission of active power.

For all the VSC ports, the control block diagram is shown in Fig. 2:

According to the classic d–q reference frame transformation and the d-axis output voltage orientation principle, the control equation for its voltage outer loop for the PQ control-based VSCs is calculated as

$$\begin{cases} i_{d,\mathrm{ref}} = \left(P^{ref}_{\mathrm{VSC}_k} - P_{\mathrm{VSC}_k}\right)\left(k_p + \dfrac{k_i}{s}\right) \\ i_{q,\mathrm{ref}} = \left(Q^{ref}_{\mathrm{VSC}_k} - Q_{\mathrm{VSC}_k}\right)\left(k_p + \dfrac{k_i}{s}\right) \end{cases} \tag{1}$$

where $P^{ref}_{\mathrm{VSC}_k}$ and P_{VSC_k} are the reference and actual values of active power of the converter VSC_k, respectively. k_p and k_i are the proportional and integral coefficients of PI control, respectively.

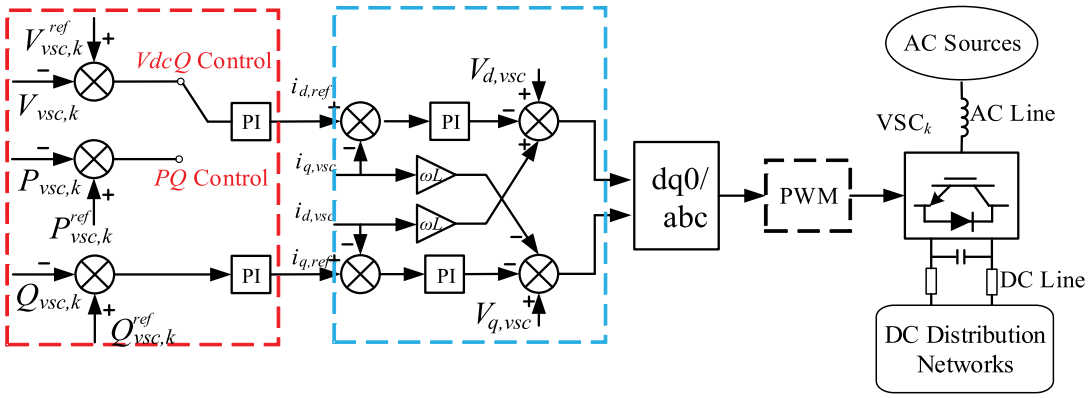

Figure 2: Block diagram of the VSC local control

For the VSCs that implement $\mathrm{V_{dc}Q}$ control, the voltage outer loop control formula can be expressed as

$$\begin{cases} i_{d,ref} = \left(V^{dc}_{\mathrm{VSC}_k} - V_{\mathrm{VSC}_k}\right)\left(k_p + \dfrac{k_i}{s}\right) \\ i_{q,ref} = \left(Q^{ref}_{\mathrm{VSC}_k} - Q_{\mathrm{VSC}_k}\right)\left(k_p + \dfrac{k_i}{s}\right) \end{cases} \tag{2}$$

where $V^{dc}_{\mathrm{VSC}_k}$ and V_{VSCK} are the reference and actual values of the DC side voltage of the converter VSC_k, respectively. k_p and k_i are the proportional and integral coefficients of PI control, respectively. For $\mathrm{V_{dc}Q}$ control and PQ control, the current inner loop is the same, which can be expressed by Eq. (3):

$$\begin{cases} v_d = V_{d,vsc} + \omega L i_{q,vsc} - \left(i_{d,\mathrm{ref}} - i_{q,vsc}\right)\left(k_p + \dfrac{k_i}{s}\right) \\ v_q = V_{q,vsc} - \omega L i_{d,vsc} - \left(i_{q,\mathrm{ref}} - i_{d,vsc}\right)\left(k_p + \dfrac{k_i}{s}\right) \end{cases} \tag{3}$$

For the application of the DC converter DCT, this study adopts the dual active bridge bidirectional DC/DC converter (DAB) structure, and its control mode is the traditional single-shift control. Its control block diagram is shown in Fig. 3:

In this study, the PI controller is used to track the active power. The shift ratio D_{DAB} is obtained by constant power control, which can be expressed as

$$D_{\mathrm{DAB_L}} = \left(P^{ref}_{DAB} - P_{DAB}\right)\left(k_p + \frac{k_i}{s}\right) \tag{4}$$

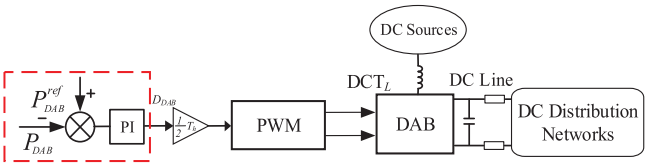

Figure 3: Control block diagram of DCT

The shift ratio of D_{DAB} is obtained by constant active control. Then, the shift angle is obtained by applying Eq. (5). Finally, the switching signal of DAB can be obtained by pulse width modulation.

$$\alpha = D_{DAB} \bullet \left(\frac{1}{2} T_h\right) \tag{5}$$

2.3 Communication Strategy

Currently, a centralized communication topology, as shown in Fig. 4, is mostly used in power distribution systems.

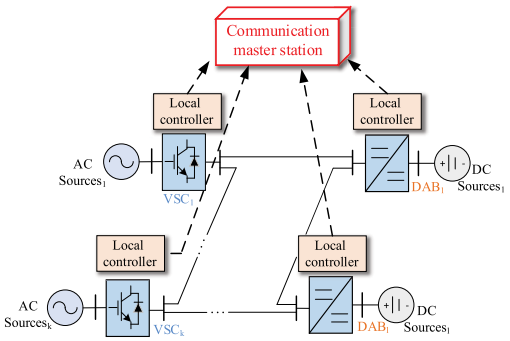

Figure 4: Diagram of a centralized communication network topology

This centralized communication topology is based on the master station. This control strategy has a simple structure and is easy to realize. However, this communication method reveals the shortcomings of poor reliability and robustness when dealing with increasingly complex distribution networks.

To solve the abovementioned problems, the distributed communication topology shown in Fig. 5 is adopted. The local controller collects data and transmits it to the local proxy controller. This local proxy controller communicates with neighboring proxy controllers, exchanges information, and then transmits the control signals to the local controller. Distributed communication requires only a sparse communication link, which is more reliable and robust than centralized communication. Therefore, a distributed communication network is used in this study. The diagram of the distributed communication network topology can be represented as follows:

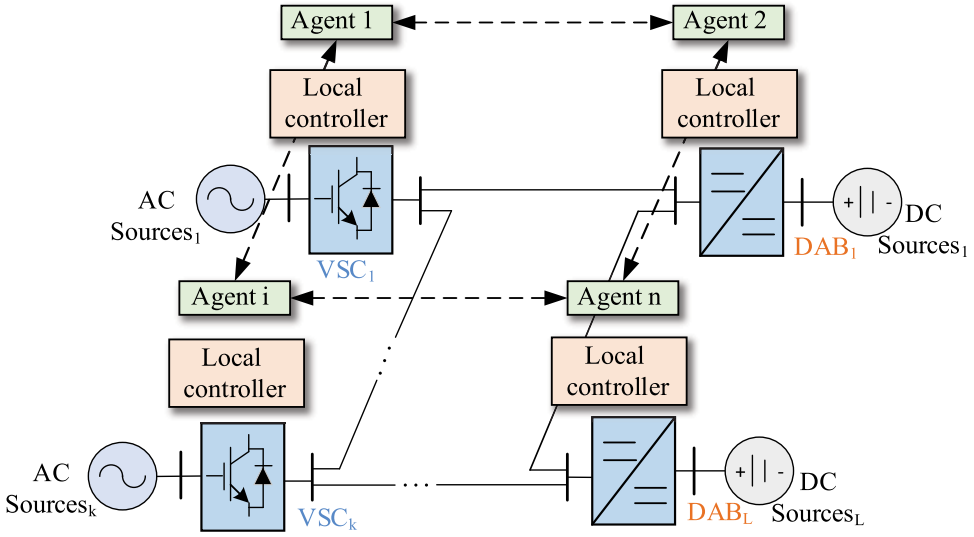

Figure 5: Diagram of a distributed communication network topology

3 Load Rate Balancing Control Based on Iterative Learning Algorithm

3.1 Preliminaries of the Communication Network

According to graph theory and multi-agent system control scheme, the communication network of a specific power distribution system can be described as a bidirectional graph G: = (V_G, E_G, A_G). Among them, V_G is the node set composed of all nodes V_G:(V_1, V_2. . ., V_3), E_G is the set of all edges $E_G \subset V_G \times V_G$, $\mathbf{A}_G$ is the adjacency matrix that describes the connection relationship of nodes, and $\mathbf{A}_G$: $\{a_{ij}\}_{n\times n}$. If communication occurs between node V_i and V_j, then $a_{ij} = 1$; if no communication occurs, then $a_{ij} = 0$. The diagram of the distributed control topology is shown in Fig. 6:

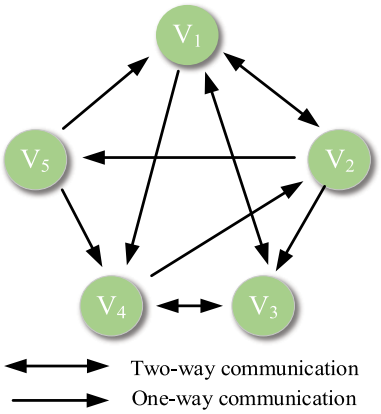

Figure 6: Diagram of a distributed control topology

The consistency algorithm based on MAS generally refers to the information interaction between an agent and neighboring agents through algorithm control. It ultimately enables a control algorithm, in which the state quantities of each intelligent agent in the system tend to be uniform. The basic formula of its

algorithm can be expressed as

$$\dot{x}_i(t) = \sum_{j \in N_i} a_{ij}\left(x_j(t) - x_i(t)\right) \tag{6}$$

where x_i represents the state quantity of the intelligent agent node, which is typically the system voltage. The frequency in this study represents the load rate. N_i is the set of adjacent nodes. $\dot{x}_i(t)$ represents the derivative of the variable.

This study improves the consistency algorithm. Specifically, by incorporating historical control experience, it becomes an ILC algorithm, which is more suitable for the AC/DC distribution system described in this study. The specific control methods will be discussed in detail in the subsequent content.

3.2 Conventional Control Strategy for Load Rate Equalization

This study presents the definition of load rate, as shown in Eq. (7):

$$\eta_i = \frac{P_i}{P_i^*} \tag{7}$$

where η_i is the load rate of the i-th branch, P_i is the actual power output on the branch, and P_i^* is the maximum power that can be output by the port power supply.

The feeder load rate indicates the proportion of the actual power on the feeder to the rated power of the feeder. To a certain extent, it can indicate whether the power distribution in the area is reasonable. The difference in load factor between feeders is used in conventional load balancing control to measure the degree of balance in power distribution.

$$\Delta\eta_{ij} = \frac{P_i}{P_i^*} - \frac{P_j}{P_j^*} \tag{8}$$

$\Delta\eta_{ij}$ denotes the difference between the load rate of feeder i and feeder j. A smaller value means more balanced power distribution among the feeders.

However, the traditional load balancing control only considers the load rate difference between feeders while ignoring the economics of feeder operation and the different distributed energy penetration rates of different feeders. Meanwhile, the traditional load balancing control usually adopts the master approach to realize load balancing, and its reliability is low. To solve the abovementioned problems, this study establishes a model of feeder load rate equalization based on the ILC control algorithm.

3.3 Load Rate Balancing Strategy Based on ILC

The expression based on the iterative learning algorithm can be described as

$$u_i(k+1) = u_i(k) + Ke_i(k) \tag{9}$$

where $u_i(k)$ represents the control input for the k-th iteration of each AC and DC port. This input is used to adjust the power output of port i. $u_i(k-T)$ is the control input for the last iteration. K is the gain matrix that needs to satisfy the convergence condition, and it is usually a diagonal matrix. $e_i(k-1)$ represents the error load rate of the previous iteration, and its definition is determined by Eq. (10):

$$e_i^{(k)} = g_i\left(\eta_{ref} - \eta_i^{(k)}\right) + \sum_{j \in N_i}\left(\eta_j^{(k)} - \eta_i^{(k)}\right) \tag{10}$$

In the formula, g_i is the flag indicating connection to the reference port; a value of 1 means that port i can be directly connected to the reference port for acquisition; 0 means otherwise. N_i is the communication set of port i, which represents all ports that have communication connections with port i. It is determined by the communication topology **G**. In addition, $\eta_i^{(k)}$ and $\eta_j^{(k)}$ are the loading rates at the k-th iteration of feeders i and j, respectively. The hierarchical control block diagram based on the iterative learning algorithm proposed in this study is shown in Fig. 7:

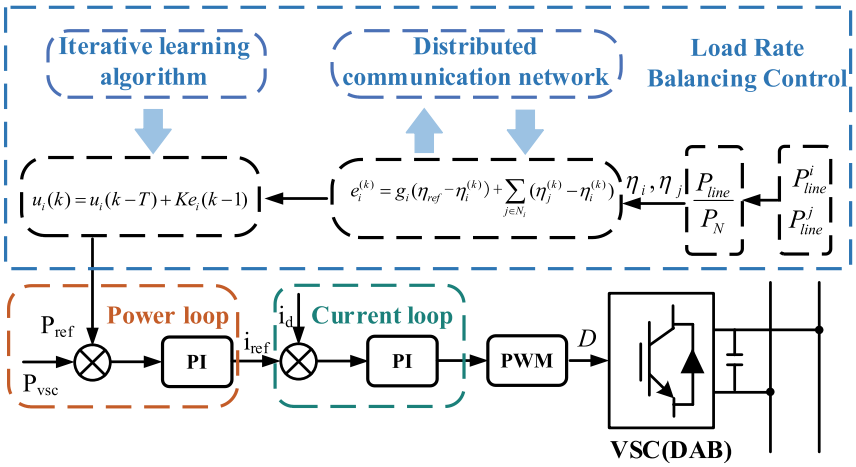

Figure 7: Block diagram of a hierarchical control system

3.4 Stability Analysis

The stability analysis of the distribution network model in this study is based on small-signal analysis. The evolution of error from one iteration to the next needs to be examined to analyze stability. First, we establish the dynamic equation of error. The load rate is a function of the actual power output P_i, and P_i is ultimately determined by the control input u_i of the ILC controller. When the iteration cycle (the time from k to $k+1$) is relatively short, the dynamic characteristics of the system from input to output within one iteration cycle can be approximated by a linear relationship. The assumption is that the change in load rate is proportional to the change in the power reference set value issued by the ILC controller:

$$\Delta\eta(k) \approx G\Delta u(k) \tag{11}$$

It can be equivalent to

$$\eta^{k+1} = \eta^k + G\left(u^{k+1} - u^k\right) \tag{12}$$

Here, G is a matrix representing the sensitivity of the load rate to changes in the control input. This matrix is determined by the underlying physical characteristics of the power grid.

The error Eq. (10) can be written in vector form as

$$e^k = -(L+B)\eta^k + B\eta_{\mathbf{ref}} \tag{13}$$

Among them, $\eta(k)= [\eta_1(k), \eta_2(k)\ldots, \eta_n(k)]^T$ is the load rate vector; L is the Laplacian matrix of the communication graph; B = diag $(b_1, b_2\ldots, b_n)$ is a diagonal matrix, which reflects which nodes are connected

to the reference node ($b_i = 1$ if connected, and $b_i = 0$ if not connected); and $\boldsymbol{\eta}_{\text{ref}}$ is a vector where all elements are the reference load rate.

Rewrite Eq. (9) in vector form:

$$u^{k+1} = u^k + Ke^k \tag{14}$$

Substitute the system dynamic Eq. (12) into the error Eq. (13);

$$\begin{aligned} e^{k+1} &= -(L+B)\,\eta^{k+1} + B\mathbf{1}\eta_{\text{ref}} \\ &= -(L+B)\left[\eta^k + G\left(u^{k+1} - u^k\right)\right] + B\mathbf{1}\eta_{\text{ref}} \end{aligned} \tag{15}$$

Substitute Eq. (14) into Eq. (15)

$$\begin{aligned} e^{k+1} &= -(L+B)\,\eta^k - (L+B)\,GKe^k + B\mathbf{1}\eta_{\text{ref}} \\ &= \left[-(L+B)\,\eta^k + B\mathbf{1}\eta_{\text{ref}}\right] - (L+B)\,GKe^k \end{aligned} \tag{16}$$

Notice that the item within the square brackets is exactly equal to e^k. Therefore, we obtain the dynamic iterative equation of the error

$$e^{k+1} = [I - (L+B)\,GK]\,e^k \tag{17}$$

where I is the identity matrix. This system is a linear iterative system. Its stability is guaranteed when the spectral radius of the matrix $I - (L + B)\,GK$ is less than 1, that is,

$$\rho\,(I - (L+B)\,GK) < 1 \tag{18}$$

A sufficient and commonly used condition is to select the learning gain matrix K such that it satisfies

$$K = \alpha\mathbf{G}^{-1} \tag{19}$$

By substituting this condition into the matrix in the convergence condition, we obtain

$$I - (L+B)\,GK = I - \alpha\,(L+B) \tag{20}$$

At this point, the stability of the system is entirely determined by the eigenvalues of the matrix $L + B$. Let λ_i be the i-th eigenvalue of the matrix $L + B$. Then, the convergence condition requires that, for all i, the following criterion is satisfied:

$$|1 - \alpha\lambda_i| < 1 \tag{21}$$

which equivalent to

$$0 < \alpha < \frac{2}{\lambda_{\max}} \tag{22}$$

where $\lambda_{\max}$ is the maximum eigenvalue of the matrix $L + B$. Given that the communication matrix $L + B$ of the system is known, an appropriate α can be selected to ensure that the selection of the gain matrix K is within a reasonable range. In this way, the spectral radius of the matrix of the linear iterative system meets the conditions, which proves the stability of the system.

4 Simulation Results and Analysis

A simulation model of a four-port AC/DC distribution network is built based on the MATLAB/Simulink software platform to verify the effectiveness of the proposed control strategy. The model comprises three AC ports and one DC port; the three AC ports use an ideal AC power supply. At the DC port, to better align with the actual situation, the power supply on the DC side is replaced by a photovoltaic and energy storage system. Among them, the photovoltaic module adopts maximum power point tracking control(MPPT), and the energy storage uses constant DC voltage control, with the DC side voltage controlled at 400 V. The maximum capacity of the four ports is the same, and the operation mode adopts the master–slave control. The third AC port is set as the master port, which adopts $V_{dc}Q$ control to control the bus voltage at the DC end. The remaining AC ports adopt PQ control, and the DC port adopts constant P control to transmit constant power. The maximum active power of all the ports is 500 kVA. The system is initially operated with DC loads, and the remaining AC loads are connected to the system at different moments. The topology diagram is shown in Fig. 8 and simulation parameters of the system is shown in Table 1.

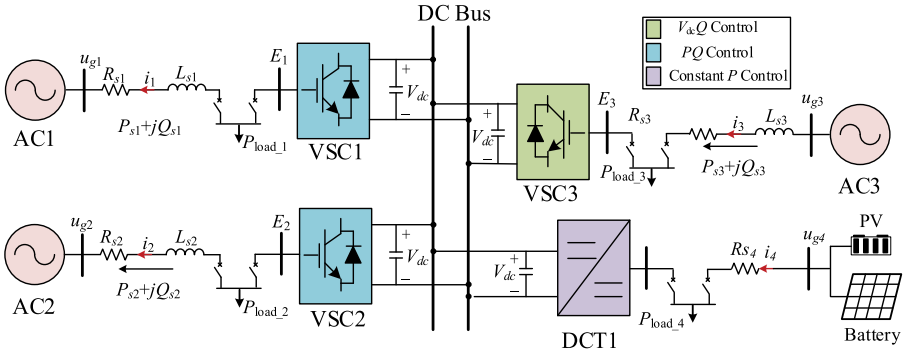

Figure 8: Topological diagram of the system simulation model

Table 1: System simulation parameters

VSC parameters	Magnitudes		
	$VSC_{1\&2}$	**VSC_3**	**DCT_1**
RLC filter	0.2 Ω/2 mH/10 μF	0.2 Ω/2 mH/15 μF	0.2 Ω/2 mH
DC capacitor C_{dc}	1000 μF	1200 μF	1500 μF
Current controller K_P/K_I	20/200	18/150	0.35/15
PLL controller K_P/K_I	0.4/2	0.5/3	/
Capacity	500 kVA	500 kVA	500 kVA
Load parameters	Magnitudes		
	$Load_1$	$Load_2$	$Load_3$	$Load_4$
Load P_{Load}/Q_{Load}	100 kW	120 kW	150 kW	30 kW
	5 kvar	10 kvar	10 kvar	
Line parameters	Magnitudes		
	Line_G1	Line_G2	Line_G3	Line_G4

(Continued)

Table 1 (continued)

VSC parameters	Magnitudes			
	$VSC_{1\&2}$	VSC_3		DCT_1
AC Line R_c/L_c	0.25 Ω/4 mH	0.25 Ω/4 mH	0.3 Ω/5 mH	0.16 Ω
Parameters of photovoltaic modules	Magnitudes			
	Parallel strings	Series-connected modules per string		Maximum power Point (25°C)
/	39	20		1.66×10^5 W
Parameters of energy storage module	Magnitudes			
	Nominal voltage	Rated capacity		LC Fillter
	480 V	47,110 Ah		5 mH/2000 μF

4.1 Case 1: General Performance of the Proposed Method

Under normal operation mode, all ports operate in accordance with the established operation mode, and the DC side voltage of the system is controlled at 1500 V. On the DC power supply side, the photovoltaic panels adopt maximum power point tracking control (MPPT), enabling them to output the maximum power. Energy storage keeps the voltage on the DC side at 400 V. The DC load is connected to the system at 0 s, and each AC load is connected to the system at 0.5, 1, and 1.5 s. The reference power of each slave control port is 0 before 3 s. After 3 s, the ILC algorithm is used to balance the load rate of each port. The simulation results are shown in Fig. 9.

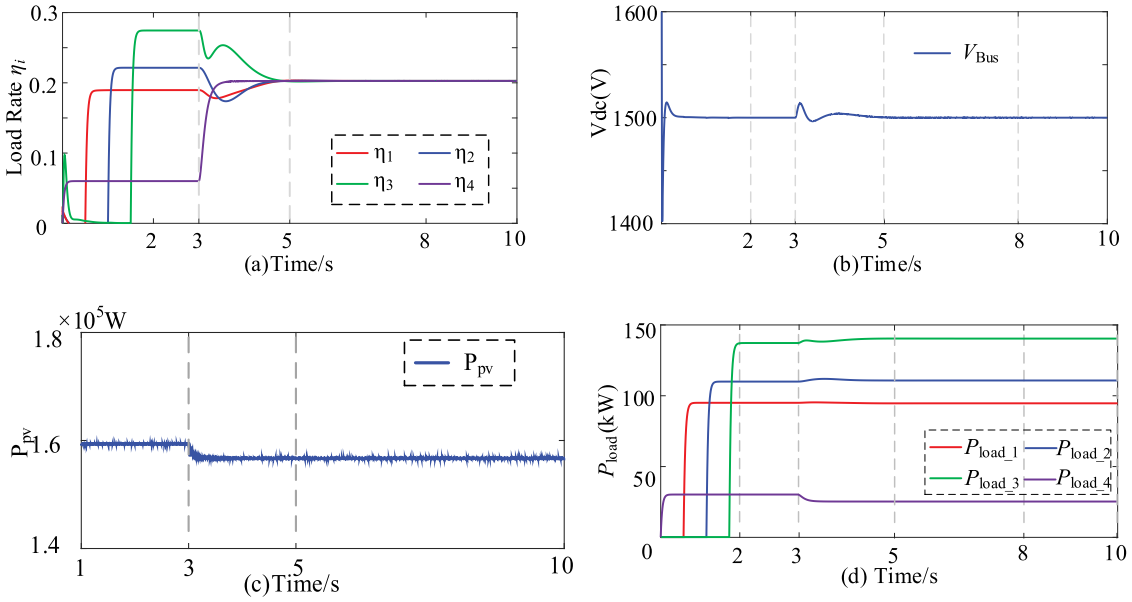

Figure 9: System simulation results under normal operation scenarios. (**a**) Load rate; (**b**) DC voltage; (**c**) P_{pv}; (**d**) P_{load}

As shown in Fig. 9, under normal simulation conditions, each load is connected to the system 2 s ago, the transmission power of each flexible interconnection device is 0 before 3 s, and the reference voltage of the DC distribution system is 1500 V. The ILC algorithm was added at 3 s, and the simulation results of the system are shown in the above figure. Fig. 9a shows the load rate schematic diagram of the four ports. It can be seen from the figure that the load rate of each port can reach the expected effect in approximately 1.5 s after the algorithm is applied. Fig. 9b shows the bus voltage of the DC distribution system. When the algorithm is added, its fluctuation is approximately 15 V, which falls within the normal fluctuation range and meets the actual requirements. Fig. 9c shows the output power of the photovoltaic module, with a maximum power of approximately 160 kW. Fig. 9d presents the load power of each port. It can be seen from the simulation results that the proposed iterative learning control algorithm can effectively balance the load rate of each port, verifying its practicability.

To explore the influence of the iterative learning gain matrix parameter K on the dynamic performance of the system, this paper further designs a parameter sensitivity analysis simulation. By setting the gain parameter K to different values respectively, we conducted a comparative simulation of the dynamic adjustment process of the load rates of the four ports, aiming to evaluate key performance indicators such as the convergence time and overshoot of the system under different control gains, thereby determining the optimal parameter range that considers both response speed and stability. Fig. 10 shows the simulation results under different K parameters.

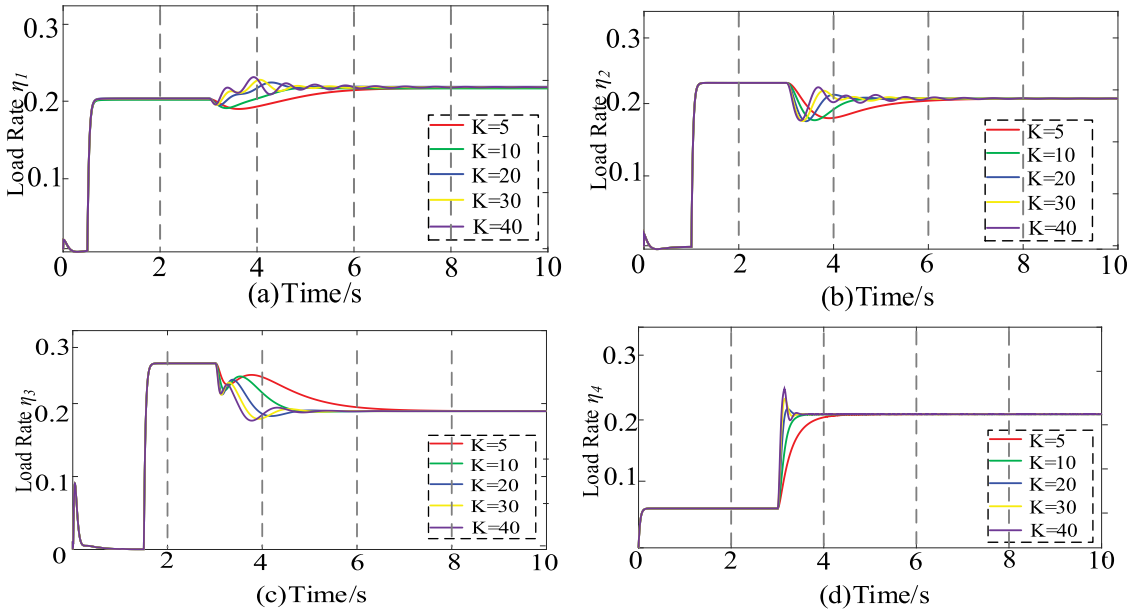

Figure 10: The load rates of each port under different parameters K. (**a**) η_1; (**b**) η_2; (**c**) η_3; (**d**) η_4

The simulation results of parameter adjustment clearly reveal the regular influence of gain K on the dynamic performance of the system. As shown in the Fig. 11, when K = 5, the system response is overly conservative. Although the overshoot is small, the convergence speed is slow and the dynamic adjustment time is too long. As the K value increases to 20, the system achieves the best balance between convergence speed and stability, enabling rapid and smooth load rate balancing with optimal dynamic performance. However, when the K value continues to increase to 30 and 50, although the convergence speed further accelerates, significant overshoot and oscillation occur, which is not conducive to the stable operation of the system. This result is consistent with the theoretical expectation in the stability analysis of Section 3.4, that

is, there exists a reasonable interval of the K value that optimizes the system performance. A small K value will lead to slow learning, while an overly large K value will disrupt the stable boundary of the system and cause oscillations. Therefore, after comprehensive consideration, K = 20 is selected as the iterative learning gain of this system.

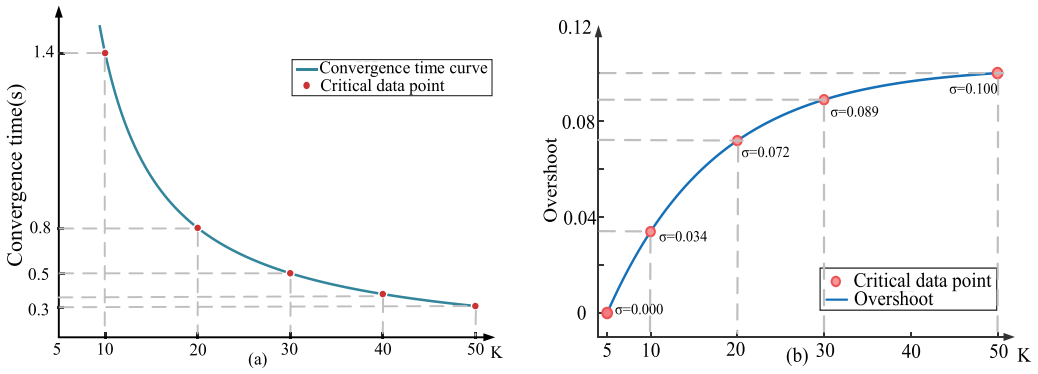

Figure 11: Convergence time and overshoot under the influence of different K values. (**a**) Convergence time; (**b**) Overshoot

4.2 Case 2: Performance under DC Side PV Fluctuation

Considering the complexity and randomness of large-scale AC/DC hybrid networks, in Case 2, we simulated the situation of photovoltaic modules at the DC side port when the light intensity and temperature changed. The light intensity changed from 1000 to 800 W/m^2 at 5 s, and the temperature rose from 25°C to 35°C at 8 s. The changes in light intensity and temperature as well as the simulation results, are shown in the following Figs. 12 and 13.

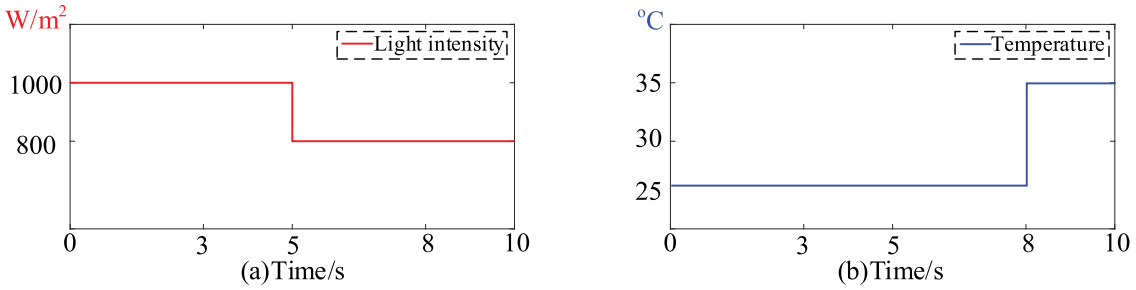

Figure 12: The situation of changes in photovoltaic conditions (**a**) Light intensity; (**b**) Temperature

As shown in the above simulation results, Fig. 13a shows the change of load rate. Due to the change of light conditions at 5 and 8 s, η_4 will drop slightly and then return to normal. Fig. 13b shows the voltage of the DC distribution system, which can be seen to have been maintained at around 1500 V all along. Fig. 13c shows the maximum power output of the photovoltaic. Due to the decrease in light intensity at 5 s, its output power will drop significantly. At 8 s, there is a relatively small increase due to the rise in temperature, which is a normal change. Fig. 13d shows the power variation of the load at each port. From the above simulation, when the DC side distributed power supply has a certain fluctuation, the algorithm proposed in this paper can still achieve the equal distribution effect of load rate, which verifies its effectiveness.

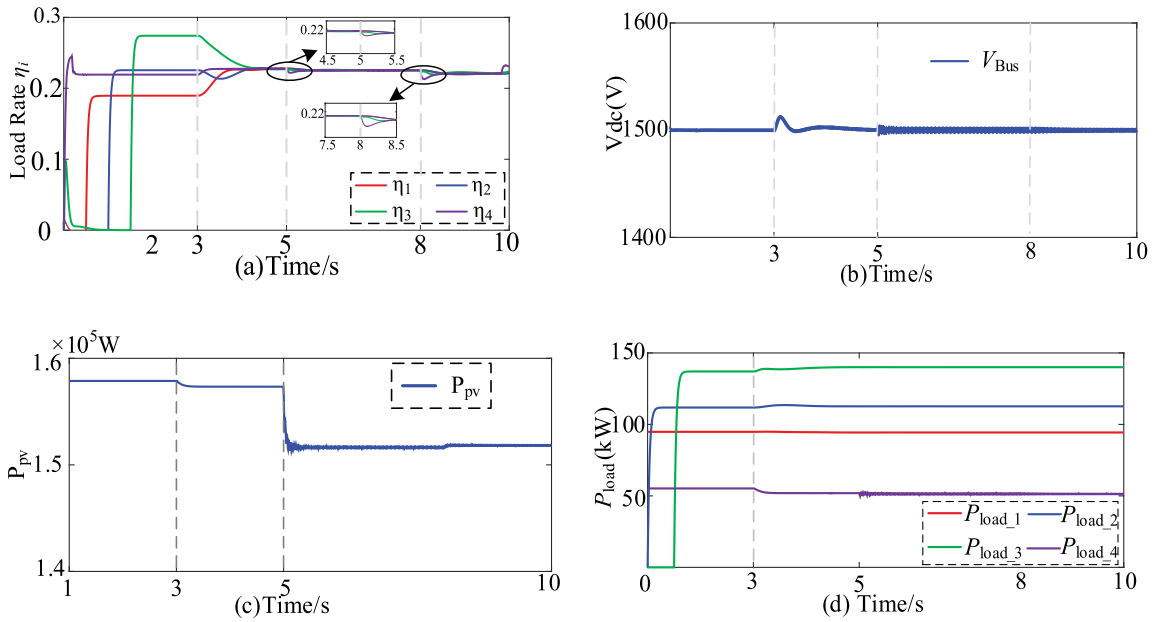

Figure 13: System simulation results under normal operation scenarios (**a**) Load rate; (**b**) DC voltage; (**c**) P_{pv}; (**d**) P_{load}

4.3 Case 3: Performance under the Fault of the VSC Ports

When a fault occurs at the slave control $port_2$, we change the control of the corresponding converter VSC_2 from PQ control to VF control, which controls the voltage and frequency of $load_2$. Thereafter, $port_2$ no longer participates in the coordinated control of all ports and is disconnected from the original communication network. The load on $line_2$ is powered solely by the converter VSC_2. The simulation results of this situation are shown in Fig. 14.

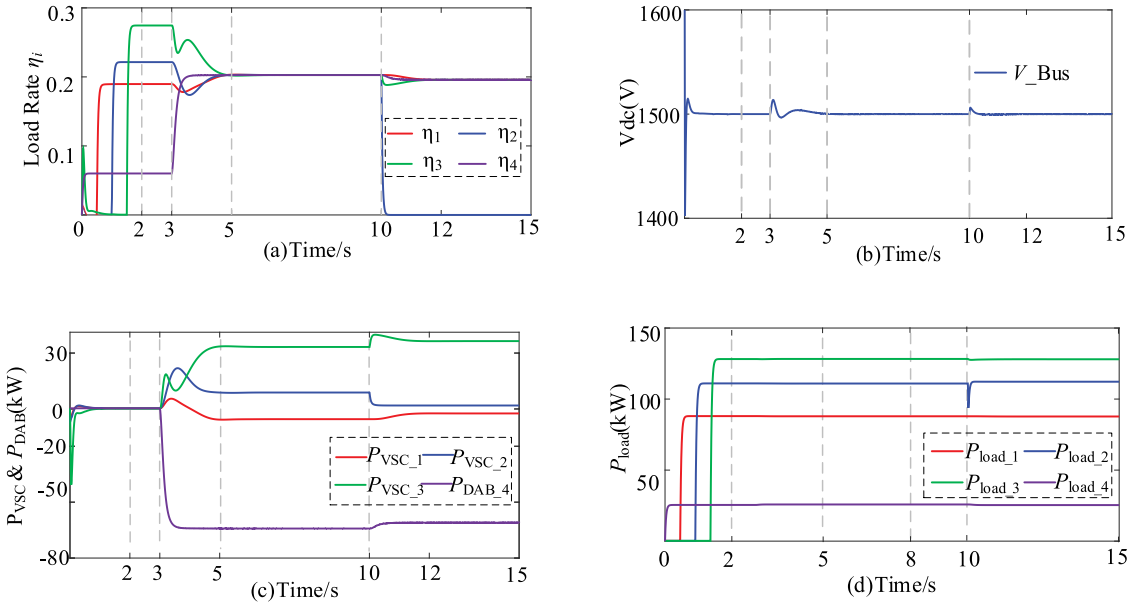

Figure 14: System simulation results under slave control port failure scenarios (**a**) Load rate; (**b**) DC voltage; (**c**) P_{VSC} & P_{DAB}; (**d**) P_{load}

From the abovementioned simulation results, at 10 s, one of the slave AC ports of the system fails and disconnects from the system. In this case, the system responds quickly to make the VSC of the corresponding port change its control strategy, and the remaining ports continue to use the original control scheme. The simulation results show that the remaining feeder load rate can remain balanced after the fault, and a slight impact on the DC voltage is observed during the switching process. In addition, after a large fluctuation in the load power of line$_2$, it quickly returns to a stable state. Therefore, the proposed algorithm in this study is effective in the case of faults.

When a fault occurs at the master control port$_3$, the control of the original main control port is switched from $V_{dc}Q$ control to VF control, which provides voltage and frequency support for the original load. In addition, a new port needs to be selected to control the voltage on the DC distribution side. In this study, we choose the first port as the new main control port and switch its control mode from PQ control to $V_{dc}Q$ control. The simulation results are shown in Fig. 15.

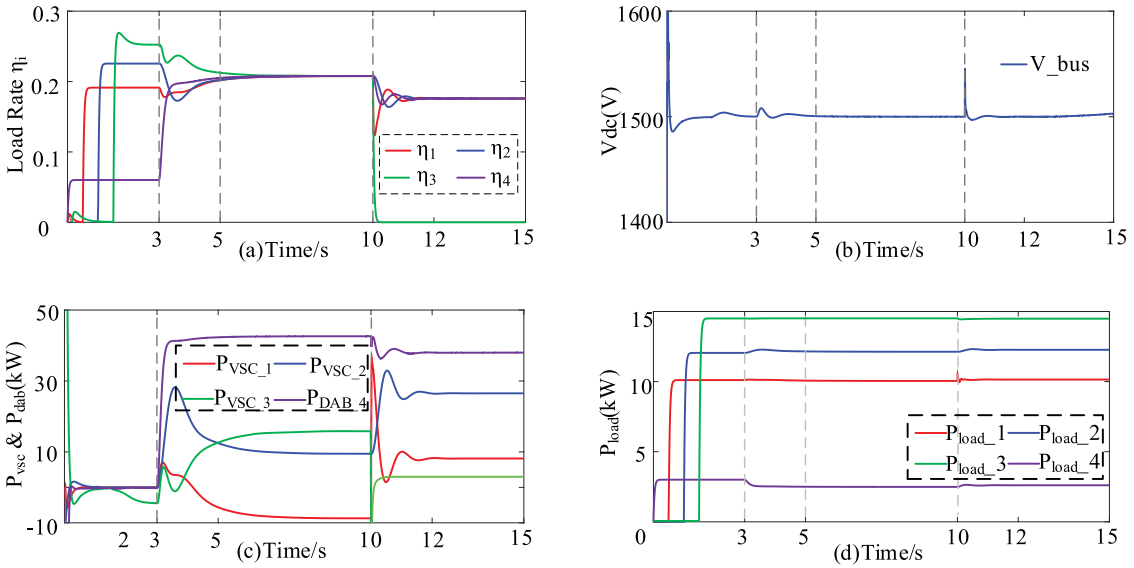

Figure 15: System simulation results under master control port failure scenarios (**a**) Load rate; (**b**) DC voltage; (**c**) P_{VSC} & P_{DAB}; (**d**) P_{load}

From the abovementioned simulation results, when the ILC algorithm is applied at 3 s, the load rates of all ports of the system converge to an equilibrium state within 2 s. At 10 s, the master control port fails and disconnects. It no longer provides power to the load, and its load rate immediately becomes 0. The remaining three ports quickly respond to the fault using the previously proposed control strategy. The load rates re-equilibrate within approximately 1 s, which restores the system to a stable operating state. Owing to the switch of the master control port, certain fluctuations will occur in the output of each flexible interconnection module and the DC voltage, which will stabilize again after the fluctuations. Therefore, the control algorithm proposed in this study remains effective even after a failure of the master control port.

4.4 Case 4: Performance Compared with Other Methods

In the current research, there are other methods to achieve load rate balancing. For instance, the event-triggered load rate adjustment method triggers control (ETC) actions by setting specific thresholds and only performs power adjustment when the load rate deviation exceeds the preset range, thereby reducing communication and control frequencies. However, this method is rather sensitive to threshold setting.

In scenarios with frequent load fluctuations or large amplitudes, it is prone to problems such as response lag or frequent triggering, leading to a decline in system dynamic performance and making it difficult to achieve rapid and smooth load balancing. In addition, the load balancing method based on the conventional consistency algorithm relies on the real-time information interaction between adjacent nodes in the system and makes the system state tend to be consistent through local coordination. This method has a simple structure and is easy to implement. However, when confronted with the strong randomness and rapid dynamic changes brought about by the high proportion of renewable energy access, its convergence speed is relatively slow, and it lacks the effective utilization of historical control experience, resulting in limited regulation efficiency under frequently changing working conditions and making it difficult to meet the requirements of modern distribution networks for rapidity and robustness.

The comparison results of the method proposed in this paper with ETC control and conventional consistency control algorithms are shown in Fig. 16.

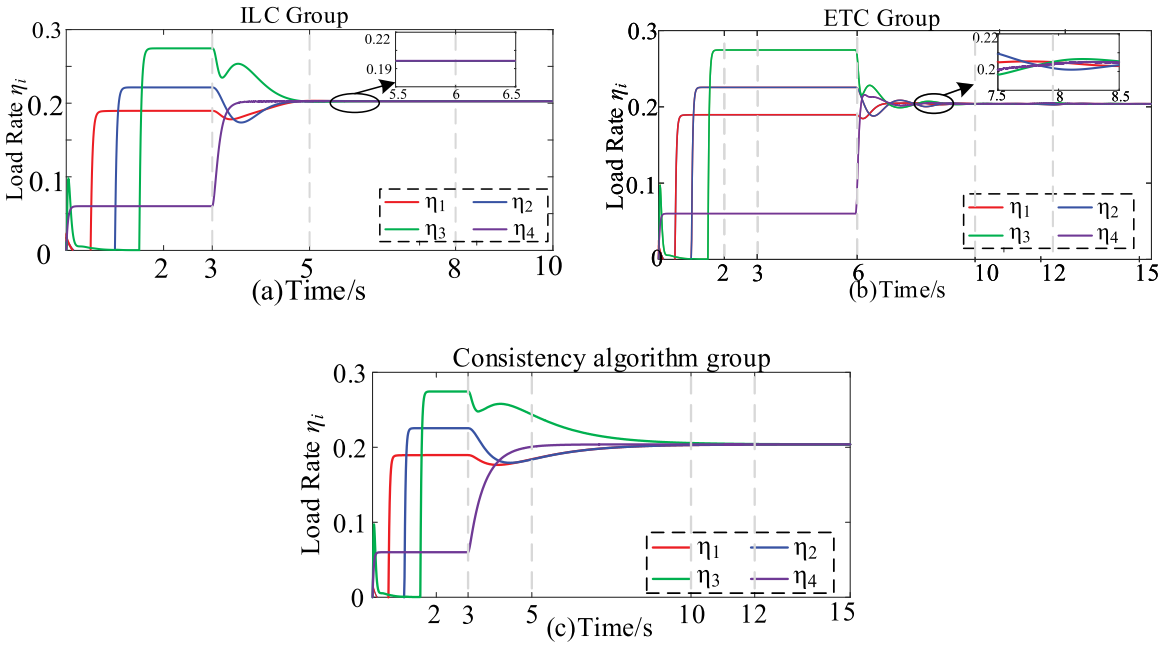

Figure 16: Comparison between the method proposed in this paper and other methods (**a**) Iterative learning control; (**b**) Event-triggered control; (**c**) Consistency algorithm control

To comprehensively evaluate the performance of the distributed iterative learning control strategy proposed in this paper, we conduct a comparative simulation with the event-triggered control method and the conventional consistency algorithm. The simulation results are shown in Fig. 16. The comparative analysis is as follows: Fig. 16a adopts the control based on the ILC algorithm proposed in this paper. Benefiting from its learning mechanism of "utilizing historical experience", the load rate of the entire system can quickly converge to the load rate balance state within approximately 1.5 s after the algorithm is implemented, and the dynamic adjustment process is smooth with a small overshoot. After entering the steady state, the load rates of each port can be stabilized around a consistent target value with minimal fluctuations, demonstrating excellent steady-state accuracy. Fig. 16b adopts an algorithm based on event-triggered control. Since the control action is only triggered when the error exceeds the threshold and the number of communications is relatively small, its control accuracy is relatively low when entering steady-state operation, and the load rate will fluctuate continuously within a certain range. Its control accuracy is

not as good as the method proposed in this paper. Fig. 16c adopts the traditional consistency algorithm, which relies on the neighborhood information interaction at the current moment and lacks the guidance of historical experience. Its convergence process shows the characteristics of gradual and slow, and it takes the longest time to reach equilibrium, making it difficult to meet the demand for rapid adjustment. Although it can eventually tend to be consistent, the convergence process is very slow in the later stage, and when subjected to continuous disturbances, the adjustment speed cannot keep up with the changes, and the anti-interference ability is relatively weak.

Comprehensive comparison shows that the ILC algorithm proposed in this paper is comprehensively superior to event-triggered control and conventional consensus algorithms in terms of convergence speed, dynamic response, steady-state accuracy, and overall robustness. It can more effectively deal with the rapid fluctuations caused by renewable energy and loads in flexible AC/DC hybrid distribution networks, and is a better solution for achieving rapid and precise load rate balance.

4.5 Case 5: Performance under Communication Time-Delay

In actual distributed communication networks, communication delay is a key factor affecting system stability and dynamic performance. To verify the robustness of the ILC algorithm proposed in this paper under non-ideal communication conditions, this study set up four different levels of communication delay scenarios, with delay parameters set at 30, 50, 100, and 150 ms respectively. The dynamic adjustment process of the load rate of the four ports in each scenario was compared and simulated. The aim is to systematically analyze the influence law of communication delay on the convergence characteristics of algorithms and the stability of systems. The simulation results are shown in Fig. 17.

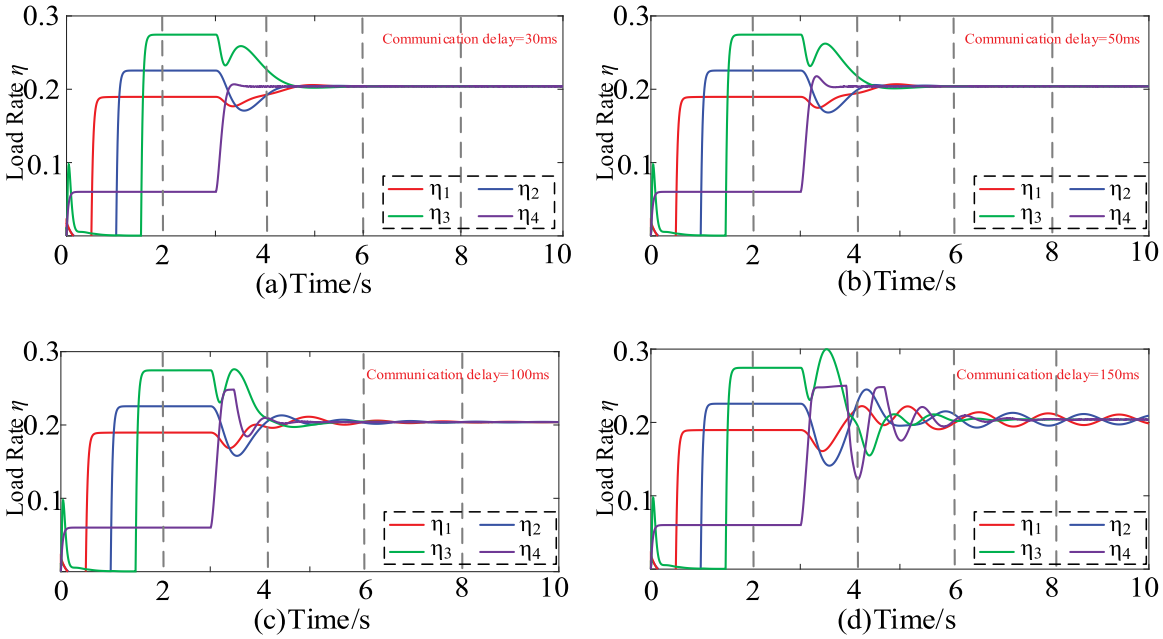

Figure 17: Load rates under different communication delays. (**a**) 30 ms; (**b**) 50 ms; (**c**) 100 ms; (**d**) 150 ms

The simulation results of the influence of communication delay show that the ILC algorithm proposed in this paper exhibits good robustness under moderate delay. When the communication delay is within the range of 30 to 50 ms, although the system load rate shows a slight lag in the initial response stage, it can still quickly converge to the balanced state, and the dynamic process is stable, indicating that the algorithm

has strong adaptability to the non-ideal conditions of light communication. However, as the delay increases to 100 ms, the convergence speed of the system slows down significantly, and an observable oscillation trend appears in the dynamic regulation process. When the delay further increases to 150 ms, the dynamic performance of the system deteriorates significantly. The convergence process is accompanied by continuous oscillation, and the adjustment time is greatly prolonged, even approaching the stable boundary. This series of simulations clearly reveals the key restrictive role of communication quality on the performance of distributed control, and verifies that the proposed ILC algorithm can maintain excellent control performance within the common engineering communication delay range (≤50 ms), providing an important parameter design basis for practical engineering applications.

5 Conclusion

This study proposes a load rate balancing strategy based on an iterative learning control algorithm to address the problem of feeder load imbalance caused by the high proportion of renewable energy access in flexible AC/DC hybrid distribution systems. This strategy integrates the consistency algorithm and ILC mechanism in the distributed communication architecture and applies this method in the field of load rate balancing for the first time. Simulation experiments were conducted through MATLAB/Simulink. The results show that the proposed method can achieve rapid convergence and balancing of the load rate, while effectively suppressing voltage fluctuations on the DC side and maintaining system voltage stability. In addition, through simulation experiments under conditions such as switching control modes when port faults occur and communication delays, the system demonstrates strong robustness and can operate continuously and reliably under both normal and fault conditions. In future research, experimental verification through the hardware-in-the-loop test platform has been identified as an indispensable subsequent step to further support these positive simulation results and promote the practical application of this technology. Moreover, the resilience algorithm and network security mechanism under communication delay and data packet loss can be further studied to improve the resilience of the system, and the multi-objective collaborative optimization direction can be developed to comprehensively improve the applicability and advancement of the method in the modern distribution system.

Acknowledgement: Not applicable.

Funding Statement: This research was funded by State Grid Anhui Electric Power Co. (No. B3120524003J).

Author Contributions: Conceptualization, [Hong Zhang]; Methodology, [Bin Xu]; Validation, [Jinzhong Li]; Writing—Review & Editing, [Xiaoxiao Meng]; Writing—Original Draft Preparation, [Cheng Qian]; Investigation, [Wei Ma]; Data Curation, [Yuguang Xie]. All authors reviewed the results and approved the final version of the manuscript.

Availability of Data and Materials: All data generated or analysed during this study are included in this published article.

Ethics Approval: This study did not involve human participants or animals, and therefore ethical approval was not required.

Conflicts of Interest: The authors declare no conflicts of interest to report regarding the present study.

References

1. Usman M, Coppo M, Bignucolo F, Turri R. Losses management strategies in active distribution networks: a review. Electric Power Syst Res. 2018;163(2):116–32. doi:10.1016/j.epsr.2018.06.005.

2. Guan Y, Wei B, Guerrero JM, Vasquez JC, Gui Y. An overview of the operation architectures and energy management system for multiple microgrid clusters. iEnergy. 2022;1(3):306–14. doi:10.23919/ien.2022.0035.
3. Jo KY, Ahn SJ, Yun SY, Choi JH. Efficient day-ahead scheduling voltage control scheme of ULTC and var of distributed generation in distribution system. IEEE Access. 2021;9:157222–35. doi:10.1109/access.2021.3129821.
4. Nasser N, Fazeli M. Buffered-microgrid structure for future power networks; a seamless microgrid control. IEEE Trans Smart Grid. 2021;12(1):131–40. doi:10.1109/tsg.2020.3015573.
5. Lu X, Lai J, Yu X. A novel secondary power management strategy for multiple AC microgrids with cluster-oriented two-layer cooperative framework. IEEE Trans Ind Inform. 2021;17(2):1483–95. doi:10.1109/TII.2020.2985905.
6. Wang J, Wang W, Yuan Z, Wang H, Wu J. A chaos disturbed beetle antennae search algorithm for a multiobjective distribution network reconfiguration considering the variation of load and DG. IEEE Access. 2020;8:97392–407. doi:10.1109/access.2020.2997378.
7. Wang J, Wang W, Wang H, Zuo H. Dynamic reconfiguration of multiobjective distribution networks considering DG and EVs based on a novel LDBAS algorithm. IEEE Access. 2020;8:216873–93. doi:10.1109/access.2020.3041398.
8. Qi Q, Long C, Wu J, Yu J. Impacts of a medium voltage direct current link on the performance of electrical distribution networks. Appl Energy. 2018;230:175–88. doi:10.1016/j.apenergy.2018.08.077.
9. Wu X, Xu Y, He J, Wang X, Vasquez JC, Guerrero JM. Pinning-based hierarchical and distributed cooperative control for AC microgrid clusters. IEEE Trans Power Electron. 2020;35(9):9865–85. doi:10.1109/tpel.2020.2972321.
10. Xie P, Jia Y, Chen H, Wu J, Cai Z. Mixed-stage energy management for decentralized microgrid cluster based on enhanced tube model predictive control. IEEE Trans Smart Grid. 2021;12(5):3780–92. doi:10.1109/tsg.2021.3074910.
11. Zhang K, Su M, Liu Z, Han H, Zhang X, Wang P. A distributed coordination control for islanded hybrid AC/DC microgrid. IEEE Syst J. 2023;17(2):1819–30. doi:10.1109/jsyst.2023.3242119.
12. Golsorkhi MS, Baharizadeh M. A unidirectional hierarchical control structure with zero power sharing error for hybrid AC/DC microgrid. IEEE Trans Energy Convers. 2023;38(1):379–91. doi:10.1109/TEC.2022.3207566.
13. Li Z, Cheng Z, Si J, Li S. Distributed event-triggered hierarchical control to improve economic operation of hybrid AC/DC microgrids. IEEE Trans Power Syst. 2022;37(5):3653–68. doi:10.1109/tpwrs.2021.3133487.
14. Ahmed M, Meegahapola L, Datta M, Vahidnia A. A novel hybrid AC/DC microgrid architecture with a central energy storage system. IEEE Trans Power Deliv. 2022;37(3):2060–70. doi:10.1109/tpwrd.2021.3103742.
15. Salman M, Ling Y, Li Y, Xiang J. Coordination-based power management strategy for hybrid AC/DC microgrid. IEEE Syst J. 2023;17(4):6528–39. doi:10.1109/jsyst.2023.3315795.
16. Rogers E, Chu B, Freeman C, Lewin P. Iterative learning control: origins and general overview. In: Iterative learning control algorithms and experimental benchmarking. Hoboken, NJ, USA: John Wiley & Sons, Inc.; 2023. p. 1–22.
17. Chen Y, Huang D, Qin N, Zhang Y. Adaptive iterative learning control for a class of nonlinear strict-feedback systems with unknown state delays. IEEE Trans Neural Netw Learning Syst. 2023;34(9):6416–27. doi:10.1109/tnnls.2021.3136644.
18. Zhai Y, Wang Y, Gu Q, Feng H, Chi R, Yao W. The secondary frequency control strategy for inland container port microgrids based on model-free adaptive iterative learning control. In: Proceedings of the 2025 IEEE 14th Data Driven Control and Learning Systems (DDCLS); 2025 May 9–11; p. 745–9. doi:10.1109/ddcls66240.2025.11065791.
19. Su H, Lai J. A novel distributed iterative learning secondary control for AC microgrids. In: Proceedings of the 2025 IEEE Industry Applications Society Annual Meeting (IAS); 2025 Jun 15–20; Taipei, Taiwan. p. 1–8. doi:10.1109/IAS62731.2025.11061620.
20. Yang Q, Chen Y, Lin Y, Chen X, Wen J. PI consensus-based integrated distributed control of MMC-MTDC systems. IEEE Trans Power Syst. 2023;38(3):2333–47. doi:10.1109/tpwrs.2022.3179530.
21. Li Y, Xu Z, Ostergaard J, Hill DJ. Coordinated control strategies for offshore wind farm integration via VSC-HVDC for system frequency support. IEEE Trans Energy Convers. 2017;32(3):843–56. doi:10.1109/tec.2017.2663664.
22. Wang P, Jin C, Zhu D, Tang Y, Loh PC, Choo FH. Distributed control for autonomous operation of a three-port AC/DC/DS hybrid microgrid. IEEE Trans Ind Electron. 2015;62(2):1279–90. doi:10.1109/tie.2014.2347913.
23. Lai J, Lu X, Wang F. Bilevel information-aware distributed resilient control for heterogeneous microgrid clusters. IEEE Trans Ind Applicat. 2021;57(3):2014–22. doi:10.1109/tia.2021.3057301.
24. Olfati-Saber R, Fax JA, Murray RM. Consensus and cooperation in networked multi-agent systems. Proc IEEE. 2007;95(1):215–33. doi:10.1109/jproc.2006.887293.